How a Dove prism transforms the orbital angular momentum of a light beam

N. González[1]**, G. Molina-Terriza**[1]**, and J. P. Torres**[1,2]

ICFO-Institut de Ciencies Fotoniques[1]*, and Department of Signal Theory and Communications*[2]*, Universitat Politecnica de Catalunya, Mediterranean Technology Park, 08860 Castelldefels (Barcelona), Spain*

noelia.gonzalez@icfo.es

Abstract: It is generally assumed that a light beam with orbital angular momentum (OAM) per photon of $l\hbar$, is transformed, when traversing a Dove prism, into a light beam with OAM per photon of $-l\hbar$. In this paper, we show theoretically and experimentally that this *OAM transformation rule* does not apply for highly focused light beams. This result should be taken into account when designing classical and quantum algorithms that make use of Dove prims to manipulate the OAM of light.

OCIS codes: (080.0080) Geometrical optics; (230.5480) prisms; (090.1970) Holography,diffractive optics

---

References and links

1. L. Allen, M. W. Beijersbergen, R. J. C. Spreeuw, and J. P. Woerdman, "Orbital angular momentum of light and the transformation of Laguerre-Gaussian laser modes," Phys. Rev. A **45** 8185 (1992).
2. G. Molina-Terriza, J. P. Torres anf L. Torner, "Management of the Angular Momentum of Light: Preparation of Photons in Multidimensional Vector States of Angular Momentum," Phys. Rev. Lett. **88**, 013601 (2002).
3. Graham Gibson, Johannes Courtial, Miles J. Padgett, Mikhail Vasnetsov, Valeriy Pasko, Stephen M. Barnett, and Sonja Franke-Arnold, "Free-space information transfer using light beams carrying orbital angular momentum," Opt. Express **12**, 5448 (2004), http://www.opticsinfobase.org/abstract.cfm?URI=oe-12-22-5448
4. R. J. Voogd, M. Singh, S. Pereira, A. van de Nes, and J. Braat, "The use of orbital angular momentum of light beams for super-high density optical data storage," OSA Annual Meeting, (Optical Society of America, 2004) paper FTuG14.
5. Lluis Torner, Juan P. Torres, and Silvia Carrasco, "Digital spiral imaging," Opt. Express **13**, 873 (2005).
6. A. Mair, A. Vaziri, G. Weihs and A. Zeilinger, "Entanglement of the orbital angular momentum states of photons," Nature **412**, 313 (2001).
7. A. Vaziri, G. Weihs and A. Zeilinger, "Experimental two-photon, three-dimensional entanglement for quantum communication," Phys. Rev. Lett. **89**, 240401 (2002).
8. G. Molina-Terriza, A. Vaziri, R. Ursin, and A. Zeilinger," Experimental Quantum Coin Tossing," Phys. Rev. Lett. **94**, 040501 (2005).
9. Julio T. Barreiro, Nathan K. Langford, Nicholas A. Peters, and Paul G. Kwiat, "Generation of Hyperentangled Photon Pairs," Phys. Rev. Lett. **95**, 260501 (2005).
10. M. Born and E. Wolf, *Principles of Optics*, Pergamon Press, 1993.
11. A. N. de Oliveira, S. P. Walborn and C H Monken, "Implementing the Deutsch algorithm with polarization and transverse spatial modes," J. Opt. B: Quantum Semiclass. Opt. **7**, 288–292 (2005).
12. J. Leach, M. J. Padgett, S. M. Barnett, S. Franke-Arnold, and J. Courtial, "Measuring the Orbital Angular Momentum of a Single Photon," Phys. Rev. Lett. **88**, 257901 (2002).
13. R. Zambrini and S. M. Barnett, "Quasi-Intrinsic Angular Momentum and the Measurement of Its Spectrum," Phys. Rev. Lett. **96**, 113901 (2006).
14. W. Chan, J.P. Torres, and J.H. Eberly, "Entanglement Migration of Biphotons in Spontaneous Parametric Down-conversion," in CLEO/QELS 2006 Technical Digest (Optical Society of America, Long Beach, California, May 2006.
15. K. T. Kapale and J. P. Dowling, "Vortex phase qubit: Generating arbitrary, counterrrotating, coherent superpositions in Bose-Einstein condensates via optical angular momentum beams," Phys. Rev. Lett. **95** 173601 (2005).

---

16. J. Courtial, D. A. Robertson, K. Dholakia, L. Allen, and M. J. Padgett, "Rotational Frequency Shift of a Light Beam," Phys. Rev. Lett. **81**, 4828 (1998).
17. M. J. Padgett and J. P. Lesso, "Dove prisms and polarized light," J. Mod. Opt. **46**, 175–179 (1999)
18. C. Cohen-Tannoudji, J. Dupont-Roc, and G Grynberg, "Atom-Photon Interactions : Basic Processes and Applications," (Wiley Science Paperback Series, 1992)
19. J. Lekner, "Polarization of tightly focused beams," J. Opt. A: Pure Appl. Opt. bf 5, 6 (2003).
20. A. T. O'Neil, I. MacVicar, L. Allen, and M. J. Padgett, "Intrinsic and Extrinsic Nature of the Orbital Angular Momentum of a Light Beam," Phys. Rev. Lett. **88**, 053601 (2002).
21. A. E. Siegman, *Lasers*, University Science Books, 1986.
22. J. Visser and G. Nienhuis, "Orbital Angular Momentum of General Astigmatic Modes," Phys. Rev. A **70**, 013809 (2004).
23. I. S. Gradshteyn and I. M. Ryzhik, *Tables of series, integrals and products*, Academic Press, 1980. We make use of some useful properties of series of Bessel functions in chapters 8-9 about Special functions.

1. Introduction

Light possesses orbital angular momentum (OAM), which is associated with the amplitude and phase of its transverse spatial profile [1]. A light beam with an azimuthal phase dependence of the type $\exp(il\varphi)$, carries an OAM per photon of $l\hbar$. In general, in the paraxial approximation, light beams can be represented as superpositions of Laguerre-Gaussian (LG) beams, or alternatively, as superposition of spiral harmonics. The weights of the superposition determine the corresponding angular momentum content of the light beam [2].

The OAM of light is receiving increasing attention as a resource, in classical and quantum optics, since the OAM exists in an inherently multidimensional space. For instance, information can be encoded into higher dimensional OAM-alphabets for its use in free space communications systems [3], and in high density optical storage in compact disks [4]. Generally speaking, the use of the OAM of light might represent a new strategy for optical imaging [5].

In quantum optics, the OAM of single and paired photons is used as a quantum resource that allows to increase the dimensionality of the working Hilbert space [2, 6], which can be used to implement new quantum applications. Illustrative examples include the violation of Bell inequalities with qutrits [7], the implementation of the quantum coin tossing protocol [8], and the generation of a quantum state in a highly multidimensional state [9].

The Dove prism is a very well known tool in optics. It acts as an image flipper in one transverse dimension, while leaving unchanged the image in the other transverse dimension. This characteristics, which makes it very useful in certain optical instruments [10], makes the OAM of a light beam to change. This property has turned Dove prims into a key element in some recent classical and quantum optics implementations that make use of the OAM of light as a resource.

A control-NOT gate, which has recently been implemented using polarization and transverse spatial modes [11], it makes use of a Dove prism located in one of the arms of an interferometer, where the spatial profile of the light beam (or photon) is properly rotated. Dove prisms are key elements of an interferometric method for measuring the orbital angular momentum of single photons [12], as well as of a scheme that allows the measurement of the orbital angular momentum content of a superposition of LG beams [13]. Recently, another interferometric method has been proposed for measuring the amount of spatial entanglement that exists between certain entangled paired photons generated in parametric down conversion [14]. A scheme to generate arbitrary coherent superpositions of OAM states in Bose-Einstein condensates makes use of Dove prism to change the handedness of light [15].

When a light beam with a well defined OAM per photon of $l\hbar$, i.e., with spatial shape in cylindrical coordinates at the beam waist $A_{in} = A_0(\rho)\exp(il\varphi)$, traverse a Dove prim, it is generally assumed that the output beam has a well defined OAM per photon of $-l\hbar$, i.e., with spatial shape $A_{out} = A_0(\rho)\exp(-il\varphi)\exp(-il\gamma)$, where $\gamma/2$ is the angle of rotation of the Dove

prism. The time dependence of the angle of rotation, and therefore the phase shift $l\gamma$, makes possible the observation of the rotational frequency shift of light beams [16]. The rotated Dove prism can also introduce polarization changes into the light beam [17].

Generally speaking, the polarization and spatial properties of light beams can not be considered separately [18]. For instance, highly focused light beams of fixed linear polarization do not exist [19]. Notwithstanding, within the paraxial regime, both contributions can be measured and manipulated separately [20].

In this paper we will show theoretically and experimentally that the OAM transformation rule $l\hbar \Rightarrow -l\hbar$ is not valid for highly focused light beams, since Dove prisms inherently introduce astigmatism, and therefore further OAM changes. Light beams with a well defined value of the OAM per photon, after traversing the Dove prism, are transformed into a superposition of states with well defined OAM. The violation of the rule $l\hbar \Rightarrow -l\hbar$, turns out to be more severe for highly focused light beams. We will provide a quantitative study of the properties of the Dove prism, by making use of the geometrical optics properties of the Dove prism, and we will verify experimentally the validity of our theoretical results in a series of experiments with a commercially available Dove prism.
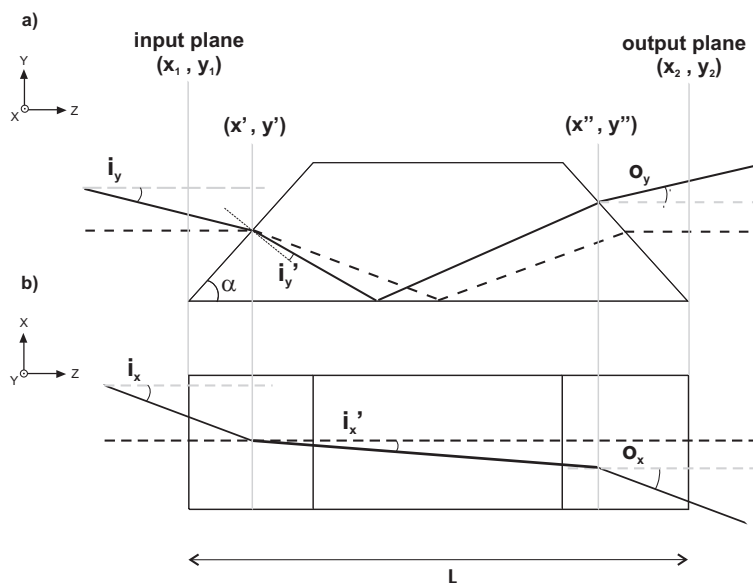

Fig. 1. Geometrical configuration of a Dove prism. (a) Lateral view ($yz-$plane) and (b) Top view ($xz-$plane). Solid and dashed lines represent the typical path of two optical rays.

2. ABCD law for a Dove prism

In Fig. 1, we present the basic geometrical configuration of a Dove prism, by showing a typical optical ray tracing. By making use of the laws of geometrical optics, one finds that the relationship between the output position (x_2,y_2) and angle (o_x,o_y) of a ray, and the input position (x_1,y_1) and angle (i_x,i_y) are given by (see appendix)

$$x_2 = x_1 + \left[\frac{L}{n} + \frac{h_0}{\tan\alpha}\left(1 - \frac{1}{n}\right) \right] i_x$$
$$o_x = i_x$$

$$y_2 = (h_0 - y_1) - h_0 \left(\frac{\eta}{n} + \frac{1}{\tan \alpha} \right) i_y$$

$$o_y = -i_y \tag{1}$$

where L is the length of the base of the Dove prism, n is the refractive index of the material, α is the base angle, and

$$h_0 = L \left\{ \tan \left[\alpha + sin^{-1} \left(\frac{\cos \alpha}{n} \right) \right] + \frac{1}{\tan \alpha} \right\}^{-1}$$

$$\eta = \frac{h_0 \sin \alpha}{L} \left[1 - \left(\frac{\cos \alpha}{n} \right)^2 \right]^{-1/2} \cos^{-2} \left\{ \alpha + sin^{-1} \left(\frac{\cos \alpha}{n} \right) \right\} \tag{2}$$

In order to derive Eqs. (1), we have made use of the paraxial approximation, so we have only kept first order terms in the angles of the optical rays. Inspection of Eqs. (1) show that the propagation of rays through the Dove prism is described by two decoupled ABCD matrices, one for each transverse dimension. We can analyze ray behaviour in each transverse coordinate separately and independently, using the appropriate ABCD matrix [21].

We have performed a series of experiments with a commercially available Dove prism (Thorlabs) to check the validity of Eqs. (1) and (2). The Dove prism parameters are $L = 63$mm, $\alpha = 45^o$ and $n = 1.51$. We use a CW He-Ne laser (wavelength 633nm). The output beam of the laser is conveniently shaped so that at the input plane of the Dove prism, the beam width is $w_0 \simeq 560 \mu$m. The beam is directed to the Dove prism by means of two mirrors to accurately control the angle and position of the beam at the input plane. The beam at the output plane of the system is demagnified to fit on a CCD camera with an appropriate imaging system.
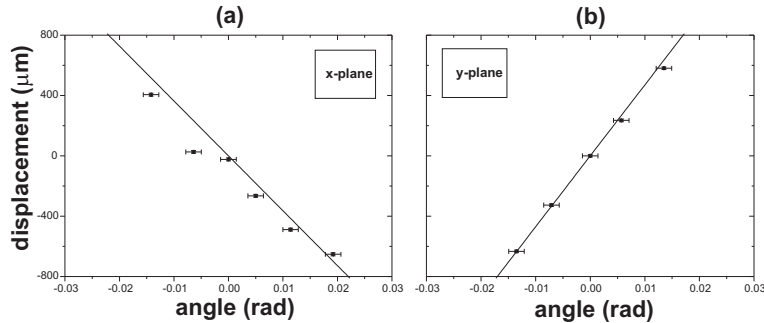

Fig. 2. Location of the center of the light beam at the output plane. (a) The angle in the x-plane (i_x) is changed. (b) The angle in the y-plane (i_y) is changed. Dots: experimental results. Solid line: theoretical results.

Figure 2(a) shows the position of the center of the beam at the output plane when the input beam, centered at $(x_1 = 0, y_1 = 0)$, propagates with different angles (i_x) at the input plane of the Dove prism. Similarly, Fig. 2(b) corresponds to the case of changing the angle i_y. The experimentally measured values agree well with the theoretical predictions as given by Eqs. (1) and (2).

3. Ellipticity induced by a Dove prism

From the ABCD matrix derived in the previous section, it is possible to calculate the effect of the Dove prism on the width and the waist position of an optical beam [21]. The important

point here is that, apart from the well known image inversion in the y direction, Eqs. (1) also show that the Dove prism modifies the beam waist position of the beam, (z_x and z_y, $z_x = z_y$), differently in both transverse dimensions. The new beam waist positions ($\bar{z}_x$ and $\bar{z}_y$) read

$$\bar{z}_x = z_x + \left[\frac{L}{n} - \frac{h_0}{\tan\alpha}\left(1 - \frac{1}{n}\right)\right]$$
$$\bar{z}_y = z_y + h_0\left[\frac{\eta}{n} + \frac{1}{\tan\alpha}\right] \tag{3}$$

The appearance of two different beam waist positions for each transverse dimension induce astigmatism in the output beam, and therefore, changes in the OAM content of the output beam [22]. Generally speaking, any optical device that introduces different optical path lengths for rays propagating in different transverse planes, should produce changes in the orbital angular momentum content of the output light beam. For the case of a Dove prism, as considered here, the difference between ray propagation in the two transverse dimensions is only noticeable for highly focused beam.

After traversing the Dove prism, the width of the light beam at the output plane is given by the well known formula for LG beams $\bar{w}_{x,y} = w_0\left[1 + (\bar{z}_{x,y}/z_0)^2\right]^{1/2}$, where w_0 is the width of the beam at the input plane and z_0 is the corresponding Rayleigh range.
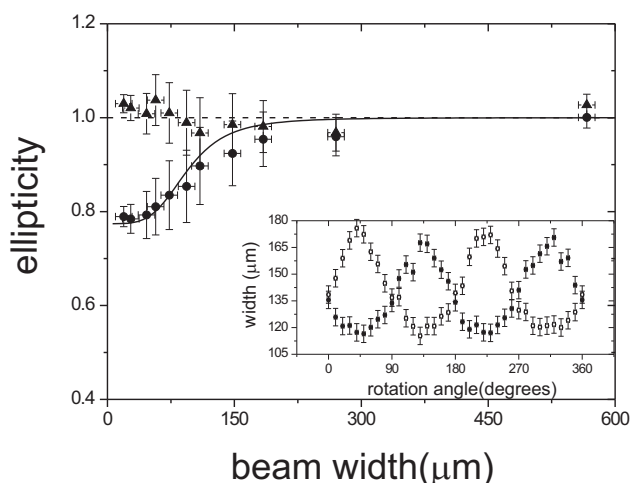

Fig. 3. Ellipticity of the output beam at the output plane, after traversing the Dove prism. Filled circles: Experimental results with the Dove prism. Triangles: experimental results when the Dove prism is removed. The solid and dashed lines are the theoretical results, as explained in the text. The dashed line corresponds to the theoretical value of the ellipticity ($e = 1$) when the Dove prism is removed. Inset: Filled circles: x-axis; Empty circles: y-axis. Input beam waist: $w_0 \simeq 50\mu$m.

Figure 3 shows the experimentally measured ellipticity at the output plane of an input gaussian beam, after traversing the Dove prim. The beam width at the input plane is changed with a series of lenses, but keeping the beam waist position at the input plane. For the measurement of the beam widths in both transverse dimensions, we have used a razor-edge measurement technique, for the two orthogonal directions. For the sake of comparison, we have also measured

the ellipticity of the output beam when the Dove prism was removed, which is also shown in Fig. 3. The theoretical curve shown in Fig. 3 corresponds to $e = (\bar{w}_x/\bar{w}_y)^2$. The inset of Fig. 3 shows how the output elliptical beam rotates when the Dove prism rotates.
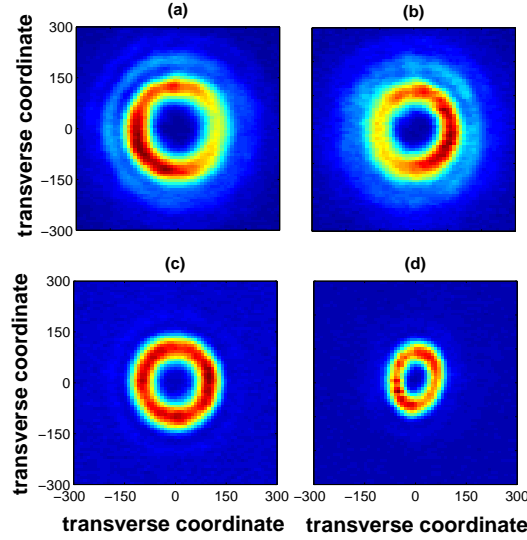

Fig. 4. Spatial light intensity measured at the output plane, with the Dove prism removed (a) and (c), and with the Dove prism, (b) and (d). (a) and (b): $w_0 = 560\mu$m, (c) and (d) $w_0 = 50\mu$m. All dimensions are in μm.

Figure 4 shows two typical spatial shape measurements obtained at the output plane, when the Dove prism is present or when it is removed. The input beam is a vortex beam with winding number $m = 2$, with two different beam widths. For very large beam widths, (a) and (b), the astigmatism induced by the Dove prism is not relevant, contrary to the case of highly focused beams, as shown in (c) and (d).

4.   OAM transformation rule of the Dove prism

The astigmatism induced by the Dove prism will transform the OAM of the output beam differently from the expected transformation $l \Rightarrow -l$. Let us consider that the input beam (at the input plane) writes $A_{in}(\rho, \varphi) \propto \rho^l \exp\left(-\rho^2/w_0^2\right)\exp(il\varphi)$, which corresponds to a LG beam with winding number l and radial index $p = 0$. The OAM of a light beam is related to the azimuthal index l, while it does not change for light beams with different index p. From Eqs. (1), the normalized beam at the output plane writes

$$A_{out}(\rho, \varphi) = N\left(\frac{x}{\bar{w}_x} + i\frac{y}{\bar{w}_y}\right)^l \exp\left(-\frac{x^2}{\bar{w}_x^2} - \frac{y^2}{\bar{w}_y^2}\right)\exp\left(i\frac{kx^2}{2\bar{R}_x} + i\frac{ky^2}{2\bar{R}_y}\right)\exp(-il\varphi) \quad (4)$$

where k is the wavenumber, N is the normalization factor and the wavefront radius of curvature reads $\bar{R}_{x,y} = \bar{z}_{x,y}\left[1 + (z_0/\bar{z}_{x,y})^2\right]$.

Due to the astigmatism induced by the Dove prism, the output beam is no longer a pure spiral harmonic with winding number $-l$, but a superposition of spiral harmonics that can be written
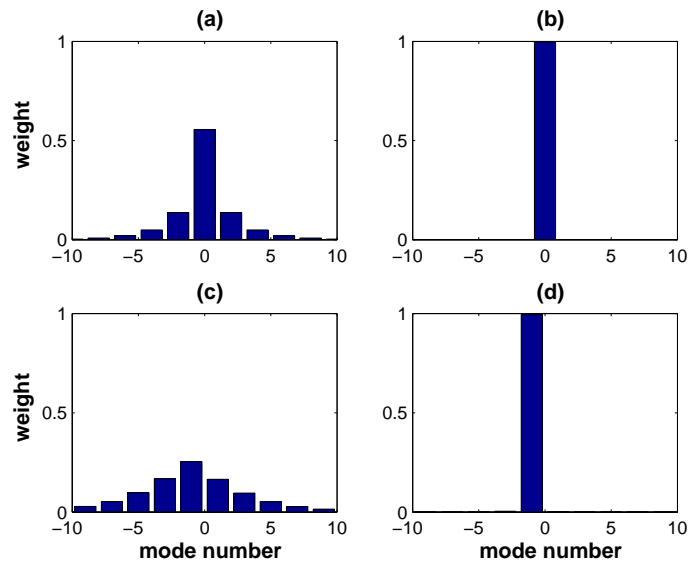
Fig. 5. OAM decomposition of the output beam. (a) Input beam width $w_0 = 20\mu$m, winding number $l = 0$; (b) $w_0 = 100\mu$m, $l = 0$; (c) $w_0 = 20\mu$m, $l = 1$; (d) $w_0 = 100\mu$m, $l = 1$.
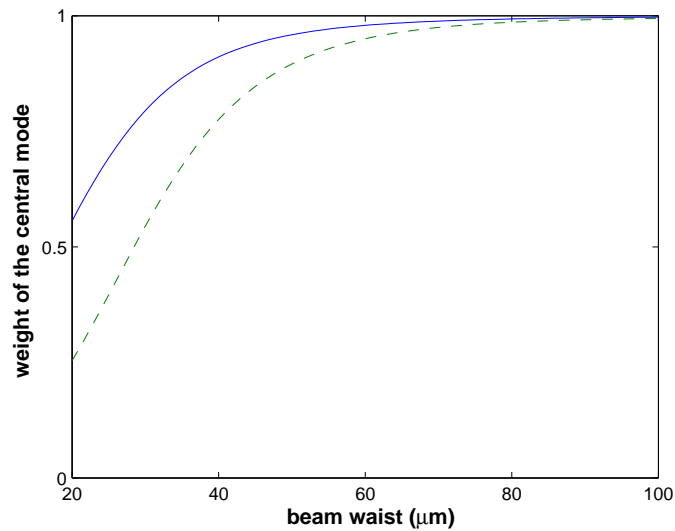

Fig. 6. Weight of the central mode of the output beam. Solid line: weight of the mode $m = 0$, for an input gaussian beam ($l = 0$). Dashed line: weight of the $m = -1$ mode, for an input $l = 1$ vortex beam.

as [2]

$$A_{out}(\rho,\varphi) = \frac{1}{(2\pi)^{1/2}} \sum_m a_m(\rho) \, \exp(im\varphi) \tag{5}$$

where $a_m(\rho) = 1/(2\pi)^{1/2} \int d\varphi A_{out}(\rho,\varphi)\exp(-im\varphi)$. The weight of the m-harmonic is given by $C_m = \int \rho d\rho |a_m(\rho)|^2$. We thus obtain [23] that the weights of the OAM superposition $\{C_m\}$ that describes the light beam, after traversing the Dove prism, is given by

$$C_m = \left(\frac{1}{2^{l-2}l!\bar{w}_x\bar{w}_y} \right) \int \rho^{2l+1} d\rho \exp\left[-\rho^2 \left(\frac{1}{\bar{w}_x^2} + \frac{1}{\bar{w}_y^2} \right) \right]$$

$$\times \left| \sum_{k=0}^{l} \binom{l}{k} i^{-k} \left(\frac{1}{\bar{w}_x} - \frac{1}{\bar{w}_y} \right)^k \left(\frac{1}{\bar{w}_x} + \frac{1}{\bar{w}_y} \right)^{l-k} J_{(l+m)/2-k}(s) \right|^2 \tag{6}$$

when $(l+m)/2$ is an integer and $C_m = 0$ otherwise. In the formula above J_m is the Bessel function of the first kind and order m, and the parameter s reads

$$s = \frac{k\rho^2}{4} \left(\frac{1}{\bar{R}_x} - \frac{1}{\bar{R}_y} \right) + i\frac{\rho^2}{2} \left(\frac{1}{\bar{w}_x^2} - \frac{1}{\bar{w}_y^2} \right) \tag{7}$$

Figure 5(a) and (b) shows the OAM decomposition of the output beam for a gaussian input beam, and Figs. 5(c) and (d) shows the corresponding OAM decomposition for a $l = 1$ vortex input beam. In all cases, the OAM decomposition of the output beam is centered at $-l$.

In Figs. 5(b) and (d), the OAM decomposition of the output beam shows a single line, so in this case Dove prism transforms the OAM of the light beam from l to $-l$. For highly focused light beams, such as it is the case of Figs. 5(a) and (c), the Dove prism transform a pure LG beam into a superposition of spiral harmonics with different OAM index.

In order to quantify the validity of the rule $l \Rightarrow -l$ to describe the OAM related behaviour of the Dove prism, Fig. 6 shows the weight of the central mode, which corresponds to $m = 0$ for the case of an input gaussian beam, and $m = -1$ for the case of a $l = 1$ input vortex beam. Generally speaking, a Dove prism performs the OAM transformation

$$l \Rightarrow \{C_m\} \tag{8}$$

where the decomposition C_m is determined by Eq. (6). For highly focused light beams, the OAM decomposition shows many modes. For larger beam widths values, the usual transformation $l \Rightarrow -l$ holds. From Fig. 6, we notice that, for a given value of the input beam width, the weight of the central mode of the OAM superposition is smaller for the case of the input vortex beam than for the gaussian beam.

5. Conclusions

We have demonstrated theoretically and experimentally that a highly focused light beam with a well defined value of the OAM per photon is transformed into a OAM superposition state when traversing a Dove prism, due to the introduction of astigmatism into the light beam propagation.

Dove prisms are being extensively used in many physical settings that make use of the OAM of light [11, 12, 13, 14, 15]. In view of the results presented here, the use of Dove prisms with highly focused beams could require the use of some compensating schemes, such as appropriate combinations of cylindrical lenses.

6. Appendix: Derivation of the ABCD matrix for a Dove prism

In this section we will derive Eqs. (1),(2) and (3), making use of the scheme shown in Fig. 1. In order to do so, one follows the rays trajectories in the figure. This is done in three steps. Firstly, we propagate the ray from the input plane to the input face of the prism $(x_1, y_1) \rightarrow (x', y')$. Secondly, we let the ray traverse the Dove prism $(x', y') \rightarrow (x'', y'')$, and finally, we calculate the ray trajectory from the output face of the prism to the output plane $(x'', y'') \rightarrow (x_2, y_2)$. The first and last steps are straightforward free-space propagations, which in our case just means finding the crossings in the three dimensional space of a straight line with a plane.

On the other hand, the middle step is divided into refraction from air to glass at the input face of the prism, reflection of the ray at the floor of the prism, and another refraction from glass to air.

The final result relates the position and angle of the ray at the input plane $(x_1, y_1; i_x, i_y)$, with those at the output plane $(x_2, y_2; o_x, o_y)$ in the following way

$$x_2 = x_1 + L \frac{\tan(i_x) + \tan(\alpha) \tan(\alpha + i'_y) \tan(i'_x)}{1 + \tan(\alpha) \tan(\alpha + i'_y)},$$

$$y_2 = L \left(\frac{\tan(\alpha) - \tan(i_y)}{1 + \tan(\alpha) \tan(\alpha + i'_y)} \right) - y_1,$$

$$o_x = i_x, \quad o_y = -i_y. \tag{9}$$

In these formulas we use the refraction angles inside the crystal $(i'_x, i'_y) = (\arcsin(\sin(i_x)/n), \arcsin(\sin(\pi/2 - \alpha - i_y)/n)$, which are shown in Fig. 1. Next, we perform a Taylor expansion to first order in the angles of these equation, since we consider the paraxial approximation regime. The result of this approximation are Eqs.(1) and (2), which we repeat here to ease the following discussion

$$x_2 = x_1 + \left[\frac{L}{n} + \frac{h_0}{\tan \alpha} \left(1 - \frac{1}{n} \right) \right] i_x$$

$$o_x = i_x$$

$$\left(y_2 - \frac{h_0}{2} \right) = - \left(y_1 - \frac{h_0}{2} \right) - h_0 \left(\frac{\eta}{n} + \frac{1}{\tan \alpha} \right) i_y$$

$$o_y = -i_y \tag{10}$$

One can note a slight variation in the formula for y_2, in order to clarify the following discussion.

A few comments are now in order. First, one notes that, although in the full equations, the output positions of a ray depend on all input angles $((i_x, i_y))$, in the linearized equations the two transverse dimensions are completely decoupled. This allows a simplification for the ABCD law, which otherwise would become a larger matrix [21]. Nevertheless, this simplification is only valid within the paraxial approximation, i.e. to first order in the incoming angles.

Secondly, Eqs.(9) show that the magnitudes of the angles are not changed in the process. This is due to the fact that the input and output media are the same (air). The change in sign of the angle in the vertical direction is due to the reflection of one ray at the floor of the prism.

Finally, we would like to mention the physical meaning of the parameter h_0, which is explicitly written in Eq.(2). It can be easily checked from the equation for y_2, that in the case of incidence angle parallel to the base of the Dove prism ($i_y = 0$), $h_0/2$ is exactly the position where the Dove prim has no effect over the ray ($y_2 = y_1 = h_0/2$).

The set of equations (10) can be directly cast into the ABCD matrix form

$$\begin{pmatrix} x_2 \\ o_x \end{pmatrix} = \begin{pmatrix} A_x & B_x \\ C_x & D_x \end{pmatrix} \begin{pmatrix} x_1 \\ i_x \end{pmatrix}, \tag{11}$$

and the corresponding one for the vertical direction. As mentioned above, due to the decoupling of the dimensions, we have one ABCD matrix for every distinct direction.

In order to use the ABCD matrix to calculate the effect of an optical system to a Gaussian beam, we have to introduce the complex radius of curvature [21] $q = (z - z_0) - i\lambda/(\pi w_0^2)$, where z is the actual longitudinal position of the beam, z_0 the position of the beam waist of the beam, λ the wavelength of the light and w_0 the beam width at the waist position. The beam can have a different complex radius of curvature for each dimension (q_x, q_y). The transformation through an optical system gives

$$\bar{q}_i = \frac{A_i + B_i q_i}{C_i + D_i q_i},$$
(12)

with $i \in \{x, y\}$, for each dimension. We can write it in this simple way, because Eqs.(10) are decoupled for the two transversal directions.

Acknowledgments